Micro-Doppler parameter estimation from a fraction of the period

Thayananthan Thayaparan, LJubiša Stanković, Miloš Daković, Vesna Popović

Abstract— **Radar micro-Doppler signatures are of great potential for identifying properties of unknown targets. All the techniques developed for extracting micro-Doppler features for the past decade rely primarily on the assumption that the time series of the signal contains at least one oscillation or more during the coherent integration time or imaging time. However, many applications in real-world scenarios involve short duration signals and often require detection and estimation of micro-Doppler characteristics. Short duration signals may contain only a fraction of an oscillation. In this paper, we develop two techniques to estimate the micro-Doppler parameters from a fraction of the period. In these scenarios, the coherent integration will cover only 1/4 and 1/2 of the oscillation. The performance of the proposed methods are evaluated using both synthetic and experimental data.**

I. Introduction

Today's radar technology has attained a broad scope of applications ranging from military to civilian. Target classification is one such area, which investigates both the moving characteristics as well as discrimination of targets. Recent research indicates that the micro-Doppler (m-D) technique exhibits a high potential for this purpose. The basic idea behind this is that mechanical vibration or rotation of a target, or structures on the target, may induce additional frequency modulations to the regular Doppler shift on the returned radar signal. This generates sidebands about the target's Doppler frequency, called micro-Doppler effect. Micro-Doppler is regarded as a unique signature and can be used to determine properties of a target. The uniqueness of micro-Doppler signatures means different micro-motions have distinct signatures [1]-[10].

Traditional techniques, such as Fourier analysis or the sliding window Fourier transform (FT) (short time Fourier transform - STFT), lack the required resolution for extracting and processing these unique m-D features. Therefore, high-resolution linear and quadratic time-frequency (TF) analysis techniques are recently employed for extracting m-D features [1]-[3], [5]-[6], [7],[9]. Several papers have been written about the ways to deal with the m-D effect. Wavelet analysis of helicopter and human data, along with the TF representation based imaging system, is presented in reference [2]. Details on the m-D effect physics, with some typical examples, are given in reference [5]. A method for the separation of the m-D effect from the radar image, based on the chirplet transform, is proposed in [7]. Both wavelet-based and chirplet-based procedures are used in reference [8] to extract m-D features such as the rotating frequency of an antenna in SAR (synthetic aperture radar) data. Recently, two techniques for the separation of a target's rigid body from m-D parts have been proposed in reference [9]. The first approach is based on order statistics of the spectrogram samples. The second approach is based on the Radon transform processing of obtained radar signals. An effective quadratic time-frequency S-method based approach in conjunction with the Viterbi algorithm to extract m-D features is proposed in [3].

All the techniques developed for the past decade rely primarily on the assumption that the time series of the signal contains at least one oscillation or more during the coherent integration time or imaging time. However, many applications in realistic real-world scenarios involve short duration signals and often require detection and estimation of micro-Doppler characteristics. Short duration signals may contain only a fraction of an oscillation. In this paper, we develop two techniques to estimate the micro-Doppler parameters from a fraction of the period. In these

scenarios, the coherent integration will cover only $\frac{1}{4}$ and $\frac{1}{2}$ of the oscillation.

II. Estimation methods

It is known that mechanical vibration or rotation on a target can induce frequency modulation on the returned radar signal and generates sidebands about the Doppler frequency shift of the target's body [4], [5]. The frequency of the returned radar signal is time dependent and can be modeled as (see Figure 1)

$$f(t) = f_0 + A\cos(2\pi f_v t + \theta), \tag{1}$$

where f_0 is the Doppler frequency caused by the target motion and $A\cos(2\pi f_v t + \theta)$ is the Doppler frequency caused by vibrating or rotating parts. Here f_v denotes the frequency of the rotation (or vibration), and θ is an arbitrary phase angle. Thus, the radar return can be written as

$$x(t) = \exp(j2\pi f_0 + j\frac{A}{f_v}\sin(2\pi f_v t + \theta)). \tag{2}$$

We will assume that the instantaneous frequency of the radar return is estimated by using the time-frequency analysis methods as described in [13], [14] giving the estimation

$$\hat{f}(t) \approx f_0 + A\cos(2\pi f_v t + \theta) \tag{3}$$

Our goal is to estimate the target rotation (or vibration) rate f_v. We will assume that the observation interval $0 \leq t < T$ is small, i.e., $2\pi f_v T < \pi$. In this case, we can not perform the conventional estimation methods for f_v (e.g., Fourier-based, zero crossing based methods, etc.). In this section, we develop two approaches to estimate the micro-Doppler parameters from a fraction of the period.

A. Estimation Method-1

In the first approach, we use 3-point model to estimate the motion parameters from a fraction of the period. Figure 1 shows the illustration of the method for frequency determination based on 3-point model. Let us consider the discrete sinusoidal signal

$$y(n) = A\sin(\omega n + \varphi), \tag{4}$$

where A is the amplitude, ω is the angular discrete frequency, and initial phase φ is the initial phase.

The frequency of the considered signal can be estimated as

$$\omega_e = \frac{1}{k}\arccos\frac{y(n-k)+y(n+k)}{2y(n)}. \tag{5}$$

Proof:

$$\frac{y(n-k)+y(n+k)}{2y(n)} =$$

$$\frac{A\sin(\omega n+\varphi-\omega k)+A\sin(\omega n+\varphi+\omega k)}{2A\sin(\omega n+\varphi)} =$$

$$\frac{2A\sin(\omega n+\varphi)\cos(\omega k)}{2A\sin(\omega n+\varphi)} = \cos(\omega k) \tag{6}$$

$$\omega_e = \frac{1}{k}\arccos(\cos(\omega k)) = \omega$$

$$= \frac{1}{k}\arccos\left(\frac{y(n-k)+y(n+k)}{2y(n)}\right) \tag{7}$$

Note that ω should be $0 \leq \omega \leq \pi/k$. This relation limits the values of lag k to several samples, which is not so important since ω is assumed to be small in this case. In this scenario, the considered time interval is much smaller than half of the period.

In the case of noisy observations

$$\hat{y}(n) = y(n) + \varepsilon(n), \tag{8}$$

where $\varepsilon(n)$ is a discrete noise. When an estimation error is introduced, Equation 5 becomes:

$$\cos(\omega k) =$$

$$\frac{y(n-k)+\varepsilon(n-k)+y(n+k)+\varepsilon(n+k)}{2y(n)+2\varepsilon(n)}. \tag{9}$$

For small $\varepsilon(n)$ compared to $y(n)$ and by using the well-known approximation $(1/(1+x) \approx 1-x$ for small $x)$ we get

$$\frac{1}{2y(n)+2\varepsilon(n)} = \frac{1}{2y(n)}\frac{1}{1+\frac{\varepsilon(n)}{y(n)}}$$

$$\approx \frac{1}{2y(n)}(1-\frac{\varepsilon(n)}{y(n)}). \tag{10}$$

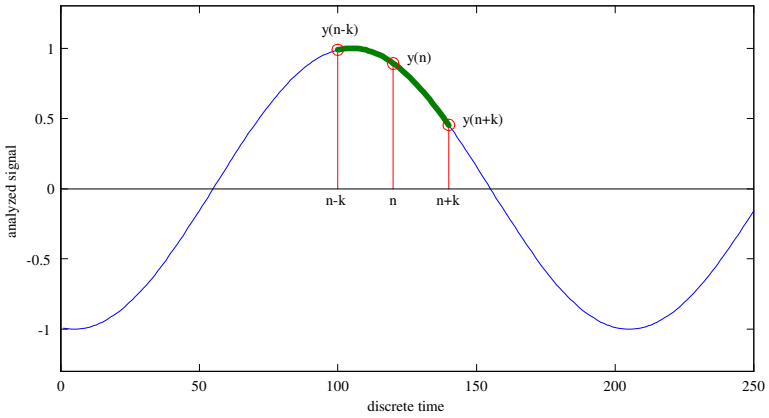

Fig. 1. Illustration of the method for frequency determination based on three points for $n = 120$ and $k = 20$

Thus, we can write

$$\cos(\omega k) = [y(n-k) + \varepsilon(n-k) + \\ + y(n+k) + \varepsilon(n+k)]\frac{1}{2y(n)}(1 - \frac{\varepsilon(n)}{y(n)}). \quad (11)$$

By neglecting the higher-order error terms such as $(\varepsilon(n)\varepsilon(n+k)$ and $\varepsilon(n)\varepsilon(n-k)$, small error multiplied by small error), the error ξ in the estimation of $\cos(\omega k)$ is:

$$\begin{aligned}\xi &= \cos(\omega k)|_{with\_noise} - \cos(\omega k)|_{without\_noise} \\ &= \frac{y(n-k)+\varepsilon(n-k)+y(n+k)+\varepsilon(n+k)}{2y(n)}(1 - \frac{\varepsilon(n)}{y(n)}) \\ &\quad - \frac{y(n-k)+y(n+k)}{2y(n)} \\ &= \left(\frac{y(n-k)+y(n+k)}{2y(n)} + \frac{\varepsilon(n-k)+\varepsilon(n+k)}{2y(n)}\right)(1-\frac{\varepsilon(n)}{y(n)}) - \\ &\quad - \frac{y(n-k)+y(n+k)}{2y(n)} \approx \\ &\approx \frac{\varepsilon(n-k)+\varepsilon(n+k)}{2y(n)} - \frac{y(n-k)+y(n+k)}{2y(n)}\frac{\varepsilon(n)}{y(n)} \quad (12)\end{aligned}$$

$$\xi = \frac{\varepsilon(n-k)+\varepsilon(n+k)}{2y(n)} - \cos(\omega k)\frac{\varepsilon(n)}{y(n)} \quad (13)$$

The mean of the estimation error is equal to zero. This means that the estimator is unbiased. The variance of ξ is equal to the mean square of the estimation error

$$var(\xi) = E[\xi^2], \quad (14)$$

where $E[\cdot]$ is the expectation operator. If we assume that $\varepsilon(n-k)$, $\varepsilon(n+k)$ and $\varepsilon(k)$ are mutually independent, the sum of three independent random variables is

$$\xi = \frac{\varepsilon(n-k)}{2y(n)} + \frac{\varepsilon(n+k)}{2y(n)} - \cos(\omega k)\frac{\varepsilon(n)}{y(n)}, \quad (15)$$

and the total variance is equal to the sum of individual variances

$$\begin{aligned}var(\xi) &= var(\frac{\varepsilon(n-k)}{2y(n)}) + var(\frac{\varepsilon(n+k)}{2y(n)}) \\ &\quad + var(-\cos(\omega k)\frac{\varepsilon(n)}{y(n)}), \quad (16)\end{aligned}$$

with

$$var(\frac{\varepsilon(n-k)}{2y(n)}) = \frac{1}{4y(n)^2}var(\varepsilon(n-k)) = \frac{\sigma_e^2}{4y(n)^2} \quad (17)$$

$$var(\frac{\varepsilon(n+k)}{2y(n)}) = \frac{1}{4y(n)^2}var(\varepsilon(n+k)) = \frac{\sigma_e^2}{4y(n)^2} \quad (18)$$

$$var(-\cos(\omega k)\frac{\varepsilon(n)}{y(n)}) = \\ = \frac{\cos^2(\omega k)}{y(n)^2}\varepsilon(n) = \frac{\cos^2(\omega k)}{y(n)^2}\sigma_e^2. \quad (19)$$

Finally the variance of ξ is:

$$\begin{aligned} var(\xi) &= \frac{\sigma_e^2}{4y(n)^2} + \frac{\sigma_e^2}{4y(n)^2} + \frac{\cos^2(\omega k)}{y(n)^2}\sigma_e^2 \\ &= \frac{\sigma_\varepsilon^2}{2y(n)^2}(1+2\cos^2(\omega k)) \\ &= \frac{(2+\cos(2\omega k))}{2}\frac{\sigma_\varepsilon^2}{y(n)^2} \\ &= \frac{(2+\cos(2\omega k))}{2}\frac{1}{SNR_n}. \end{aligned} \quad (20)$$

where SNR_n is signal-to-noise ratio at the time instant n and we assume that noise samples $\varepsilon(n-k)$, $\varepsilon(n)$ and $\varepsilon(n+k)$ are independent with variance σ_ε^2. For small ωk, $\cos(2\omega k) \approx 1$ and we finally get

$$var(\xi) \approx \frac{3}{2}\frac{1}{SNR}. \quad (21)$$

The most significant component of the noise is related to the discretization error in the estimation of the instantaneous frequency using the discrete frequency grid. The simplest way to reduce this error is by using several points, n, and several lags, k, to obtain set of estimates

$$\Omega = \{\omega_{e,n,k}\}, \quad (22)$$

and the resulting estimate, that is, the mean value of such estimates is,

$$\hat{\omega}_e = \underset{\omega_{e,n,k}\in\Omega}{mean}\ \omega_{e,n,k}. \quad (23)$$

Assuming that estimations $\omega_{e,n,k}$ are statistically independent, the variance of the resulting estimation error is

$$var(\xi_e) = \frac{var(\xi_{e,n,k})}{N_\Omega}, \quad (24)$$

where N_Ω is number of independent estimations, i.e. the number of elements of the set Ω.

B. Estimation Method-2

In the second approach, we use cubic polynomial fitting to estimate the motion parameters from a fraction of the period. Let us consider the signal of the form

$$y(n) = A\sin(\omega n + \varphi) + B, \quad (25)$$

with $\omega \ll 1$. The signal can be expanded into Taylor series around $n = 0$ as

$$y(n) = y(0) + \frac{y'(0)}{1!}n + \frac{y''(0)}{2!}n^2 + \quad (26)$$

$$+\frac{y'''(0)}{3!}n^3 + \cdots = A\sin(\varphi) + B + A\omega\cos(\varphi)n -$$

$$-\frac{A\omega^2\sin(\varphi)}{2}n^2 - \frac{A\omega^3\cos(\varphi)}{6}n^3 + \ldots \quad (27)$$

where n is a continuous variable. It is known that the Taylor expansion is the best polynomial expansion of the analyzed signal at $n = 0$. Let us now approximate the signal $y(n)$ with cubic polynomial

$$\hat{y}(n) = p_0 + p_1 n + p_2 n^2 + p_3 n^3 \quad (28)$$

where coefficients p_k are chosen in order to minimize the total approximation error over the whole considered time interval. Note, an unknown initial phase appears as $\sin(\varphi)$ in the even terms and as $\cos(\varphi)$ in the odd terms for the exponent n of a polynom $y(n)$.

If we divide the coefficient of n^2 by the constant term we obtain

$$\frac{-\frac{A\omega^2\sin(\varphi)}{2}}{A\sin(\varphi) + B} \quad (29)$$

and, for sinusoid offset $B = 0$, we get

$$\frac{-\frac{A\omega^2\sin(\varphi)}{2}}{A\sin(\varphi)} = \frac{-A\omega^2\sin(\varphi)}{2A\sin(\varphi)} = -\frac{\omega^2}{2}. \quad (30)$$

On the other hand, if we use coefficients of n and n^3 there is no need to have $B = 0$ since we have

$$\frac{-\frac{A\omega^3\cos(\varphi)}{6}}{A\omega\cos(\varphi)} = \frac{-A\omega^3\cos(\varphi)}{6A\omega\cos(\varphi)} = -\frac{\omega^2}{6}. \quad (31)$$

According to equations 27 and 28, we can now estimate the frequency of the considered signal (for $B = 0$) as

$$\frac{p_2}{p_0} = -\frac{\omega^2}{2} \quad (32)$$

and we obtain

$$\omega_{estimated} = \hat{\omega}_1 = \sqrt{-\frac{2p_2}{p_0}}. \quad (33)$$

Similarly, but without the assumption of $B = 0$, we get

$$\frac{p_3}{p_1} = -\frac{\omega^2}{6} \tag{34}$$

and the estimation is

$$\omega_{estimated} = \hat{\omega}_2 = \sqrt{-\frac{6p_3}{p_1}}. \tag{35}$$

Let us now consider the case with $2N + 1$ samples of the analyzed signal obtained for $-N \leq n \leq N$. The total approximation error is

$$e = \sum_{n=-N}^{N} |y(n) - \hat{y}(n)|^2, \tag{36}$$

where coefficients p_k are determined by minimizing e, i.e., by solving

$$\frac{\partial e}{\partial p_k} = 0 \tag{37}$$

for $k = 0, 1, 2, 3$.

Now the estimation error can be calculated as

$$\omega - \hat{\omega}_2 = \left(\frac{N^2 + N}{36} + \frac{1}{24}\right)\omega^3 + O(\omega^5) \tag{38}$$

Note that for small ω and $\omega N < 1$ the estimation error is small. For example, if we have $2N + 1 = 65$ samples of the sinusoidal oscillation with period $T = 256$, we get $\omega = \pi/128$. In this example we know the true frequency. When we approximate the data set with cubic polynom, we can find coefficients p_1 and p_3 and estimate $\hat{\omega}_2$. We can then calculate the estimation error $\omega - \hat{\omega}_2$. In this example, the estimation error is then $\omega - \hat{\omega}_2 = 0.00043$ with relative error of 1.8%. It should be noted in this example that the signal is 1/4 of the period of the analyzed sinusoid. We can even define a better estimator according to (38)

$$\hat{\omega}_3 = \hat{\omega}_2 + \left(\frac{N^2 + N}{36} + \frac{1}{24}\right)\hat{\omega}_2^3 \tag{39}$$

Here we replace the true frequency ω in the estimation error with the estimation $\hat{\omega}_2$.

III. Simulation

A. Example 1

Let us consider the discrete signal

$$y(n) = A\sin(\omega n + \varphi) \tag{40}$$

with simulation parameters $A = 0.9$, $\omega = 0.03$, $\varphi = 1.27$, $-32 \leq n \leq 32$. Let the signal be discretized over the interval $[-1, 1]$ with $M = 128$ discretization levels

$$y_D(n) = \frac{2}{M}\left[\frac{M}{2}y(n)\right] \tag{41}$$

where $[\cdot]$ denotes the nearest integer. Now choose $n = 0$ and perform the frequency estimation according to (5) for various values of lag k.

Figure 2 shows the analyzed signal and estimation results using Method-1. Figure 2a and Figure 2d illustrate an example with $M = 512$ discretization levels. Since the discretization noise estimation is inaccurate for small k, the highest possible lags k are used for the frequency estimation. The mean estimate over the range of lag $16 \leq k \leq 32$ is $\hat{\omega}_e = 0.0300$ with the relative error 0.01%. The estimation method-2 gives $\hat{\omega}_2 = 0.0291$ with the relative error 3.10%. After the correction according to (39), $\hat{\omega}_3 = 0.0298$ with the relative error 0.70%. Less than 5 percent error from the true value can be considered to be accepted value. More examples will be provided in this section.

The experiment is repeated with $M = 128$ discretization levels. Results are presented in Figure 2b and Figure 2e. The mean estimate over the range of lag (in time) $16 \leq k \leq 32$ is $\hat{\omega}_e = 0.0299$. The relative error of the mean estimate over the range of lag $16 \leq k \leq 32$ is 0.36%. The estimation method-2 gives $\hat{\omega}_2 = 0.0289$ with the relative error 3.70%. After the correction according to Equation (39), we get $\hat{\omega}_3 = 0.0296$ with the relative error 1.34%.

Figure 2c and Figure 2f illustrate the case with $M = 32$ discretization levels. The mean estimate over the range of time lag $16 \leq k \leq 32$ is $\hat{\omega}_e = 0.0295$. The relative error of the mean estimate over the range of time lag $16 \leq k \leq 32$ is 1.7%. The estimation method-2 gives $\hat{\omega}_2 = 0.0288$ with the relative error 4.09%. After correction according to (39), we

obtain $\hat{\omega}_3 = 0.0295$ with the relative error 1.74%. These results show that when the number of discretization levels is high, both methods are in good agreement with true value. When there is limited number of discretization levels, the estimation method-1 provides reliable results at higher time lags while the estimation while method-2 provides consistent results. The estimation method-2 requires more data in order to perform accurate cubic polynomial approximation.

B. Example 2

Let us now consider the sinusoidally frequency modulated signal of the form

$$x(t) = \exp(j64\sin(2\pi t - \frac{\pi}{3})) + \varepsilon(t) \quad (42)$$

over time interval $0 \leq t < 250\,\text{ms}$ sampled with $T = 1/512$. Assume the modulation frequency is 1 Hz. The discretized signal is of the form

$$x(n) = \exp(j64sin(\frac{2\pi}{512}n - \frac{\pi}{3})) + \varepsilon(n), \quad (43)$$

with $0 \leq n < 128$, where $\varepsilon(n)$ is the Gaussian white noise with variance σ_ε^2.

Figures 3a,b,c illustrate the results with $\sigma_\varepsilon^2 = 0$. We use the S-method in order to obtain the time-frequency representation of the analyzed signal (Figure 3a) [11]. The instantaneous frequency is estimated by using the maximum position of the time-frequency representation and is shown in Figure 3b. Here we can see the effect of discretization. The estimation of the modulation frequency is calculated using the estimation method-1 (Figure 3c). The mean estimate over the range of lag $40 \leq k \leq 63$ is $\hat{\omega}_e = 2\pi \cdot 0.99\,\text{Hz}$. The estimation method-2 gives $\hat{\omega}_2 = 2\pi \cdot 1.023\,\text{Hz}$. Figure 3d,e,f illustrate the results for $\sigma_\varepsilon^2 = 1$ i.e., for SNR=0 dB. The mean estimate over the range of lag $40 \leq k \leq 63$ is $\hat{\omega}_e = 2\pi \cdot 1.05\,\text{Hz}$. Using method-2, the estimated frequency is $\hat{\omega}_2 = 2\pi \cdot 1.09\,\text{Hz}$. These results show that at high SNR, the estimation method-2 provides reliable results and the estimation method-1 provides reliable results at higher time lags. At low SNR, the estimation method-1 provides better results at higher time lags while the estimation method-2 provides the results, where the accuracy is within 9 percent error from the true value. These results suggest that the estimation method-2 is sensitive to high noise level.

C. UH-1D Helicopter

In this example we consider the simulated signal of a German Air Force Bell UH-1D Helicopter known also as 'Iroquois'. The simulation is performed according to [4]. Several effects are emphasized in the TF representation of Figure 4a. The stationary patterns along the time-axis correspond to the rigid body reflection, the vibration of the target or the radar-clutter caused by the movement in the target background. The motion of the two main blades is modeled by two rotating reflectors, producing sinusoidal FM signals with a large magnitude in the frequency direction. The main rotor flashes are simulated by the signals producing lines connecting peaks of the sinusoidal FM signal with time axis. The smaller pulses that can be seen in Figure 4a correspond to the tail rotor flashes. These flashes correspond to periodic alignment of the main and tail rotors to maximally reflect the radar signal. Note that other effects that can be observed in a radar image, including multipath, are not considered here.

Therefore, the simplified model of the reflected UH-1D signal can be written as:

$$x(t) = x_{RIG}(t) + x_{ROT}(t) + x_{FL_M}(t) + x_{FL_T}(t), \quad (44)$$

where $x_{RIG}(t)$, $x_{ROT}(t)$, $x_{FL_M}(t)$ and $x_{FL_T}(t)$ represent signals caused by the rigid body, rotation of the main rotor, and the main and tail rotor flashes, respectively. The signal is considered within the interval of 400 ms, sampled with a rate of $\Delta t = 1/48000\,\text{s}$. Four sinusoidal components, caused by the rigid body, are at the frequencies $-10.3\,\text{kHz}$, $-2.5\,\text{kHz}$, $2.3\,\text{kHz}$ and $2.7\,\text{kHz}$. Two components at $-0.4\,\text{kHz}$ and $0.4\,\text{kHz}$ correspond to the modulated time tones commonly added to the data tape [12]. The sinusoidal FM signals, corresponding to the rotation of the main rotor blades, are modeled as:

$$x_{ROT}(t) =$$

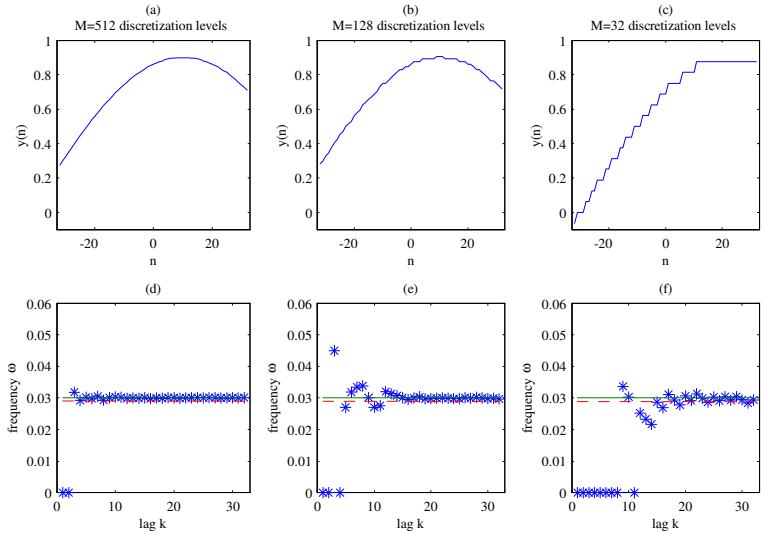

Fig. 2. Analyzed signal discretized with (a) 512 levels, (b) 128 levels, and (c) 32 levels. Estimation results for various lags k are obtained with (d) 512 levels, (e) 128 levels, and (f) 32 levels. The solid line represents the true value, asterisk represents the values estimated by method-1, and the dashed line represents the value estimated by method-2.

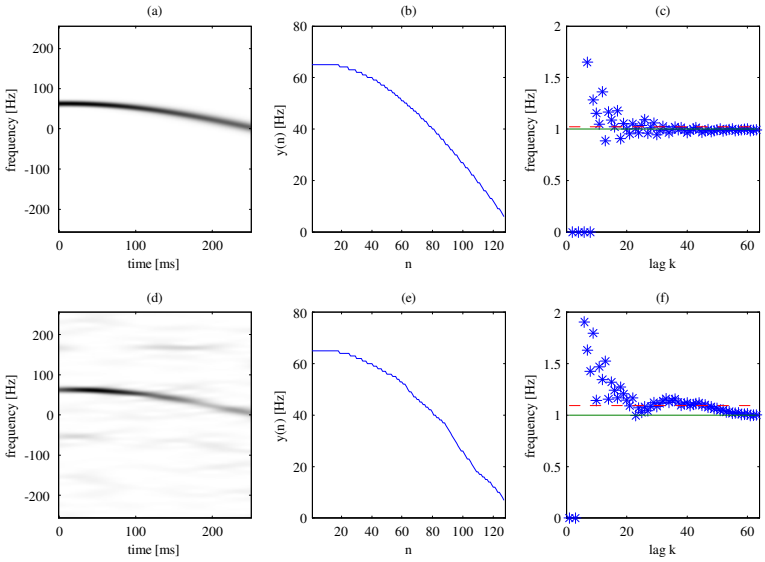

Fig. 3. Noiseless case: (a) time-frequency representation of the analyzed signal, (b) the instantaneous frequency of the signal, and (c) estimation results for various lags k. Noise case: (d) time-frequency representation of the analyzed signal, (e) the instantaneous frequency of the signal, and (f) estimation results for various lags k. The solid line represents the true value, asterisk represents the values estimated by method-1, and the dashed line represents the value estimated by method-2.

$$= \sigma_{ROT}[\exp(j2\pi A_{ROT}\sin(2\pi t/T_{ROT}))+ + \exp(-j2\pi A_{ROT}\sin(2\pi t/T_{ROT}))] \quad (45)$$

where $T_{ROT} = 175\,\text{ms}$ and $A_{ROT} = 19\,\text{kHz}$. The main and tail rotor flashes are modeled as broadband pulses given as:

$$x_{FL_M}(t) = = \sigma_{FL_M}\sum_k \delta(t - kT_{ROT}/2) *_\tau h_{FL_M}(t) \quad (46)$$

$$x_{FL_T}(t) = = \sigma_{FL_T}\sum_k \delta(t - kT_{TAIL}/2) *_\tau h_{FL_T}(t), \quad (47)$$

where T_{TAIL} in our experiment is $T_{TAIL} = 35.8\,\text{ms}$, while $h_{FL_M}(t)$ and $h_{FL_T}(t)$ are cut-off filters given in the frequency domain as:

$$H_{FL_M}(\omega) = \begin{cases} 1 & |\omega| < 2\pi A_{ROT} \\ 0 & \text{elsewhere,} \end{cases} \quad (48)$$

$$H_{FL_T}(\omega) = \begin{cases} 1 & 7.35\,\text{kHz} < \dfrac{\omega}{2\pi} < 15.7\,\text{kHz} \\ 0 & \text{elsewhere.} \end{cases} \quad (49)$$

The signal is corrupted with the Gaussian noise. The SNR in this case is 3 dB. To compare our simulated radar image with the real one, refer to [4], [12].

In order to demonstrate our estimation methods, we have extracted a part of the helicopter data signal, which is presented in Figure 4b. The resulting instantaneous frequency estimation is shown in Figure 4c and the estimated frequency for various lag k is shown in Figure 4d. The mean estimated rotation per minute (rpm) over the range of lag $15 \le k \le 35$ is $\hat{\omega}_e = 352$. The estimation method-2 gives $\hat{\omega}_2 = 362$. The true value is 343 rpm. It should be noted that part of the discrepancy in the estimation value is caused by the noise and rigid body part (i.e., the horizontal line in the TF at approximately -5 kHz), which cause inaccurate IF estimation between n=53 and n=60 in Figure 4c.

We have repeated the procedure with different time instant n. In this case, two window sizes, narrow and wide windows, are used. The procedure is performed without additional noise and with additional noise. Results are presented in Figure 5 for noisy signals. Mean estimated rpm values using method-1 are 338 and 323 for the narrow and wide windows, respectively. Using method-2, mean estimated rpm values are 328 and 329 for the narrow and wide windows, respectively.

In Figure 6, results are presented for signals without additional noise. Mean estimated rpm values using method-1 are 349 and 348 for the narrow and wide windows, respectively. Using method-2, mean estimated rpm values are 329 and 330 for the narrow and wide windows, respectively. Both methods are in good agreement with the true value.

IV. Experimental data analysis

A. Rotating fan

Experimental trials were conducted to investigate and determine the m-D radar signatures of objects that could be found in indoor radar imaging. The object in these experiments is rotating fan data supplied to us by Prof. Moeness Amin, Villanova University. The rotational motion of blades in a fan imparts a periodic modulation on radar returns. The rotation-induced Doppler shifts relative to the Doppler shift of the body occupy unique locations in the frequency domain. Whenever a blade has specular reflection such as at the advancing or receding point of rotation, the particular blade transmits a short flash or periodic modulation to the radar return. The rotation rate of the blade is directly related to the time interval between these flashes. The duration of a flash is determined by the radar wavelength and by the length and rotation rate of the blades. A flash resulting from a blade with a longer length and radar with a shorter wavelength will have a shorter duration.

The fan in this experiment is rotating at a height of approximately 2 m and at a range of 3 m from the radar. The fan has 4 metallic blades. The rotation rate of the blades is known to be 1050 rpm for this data. The experiment was conducted with the radar operating at frequency of 903 Hz. The sampling frequency is 5000 Hz.

Figure 7 illustrates the results. In order to demonstrate our estimation methods, we have

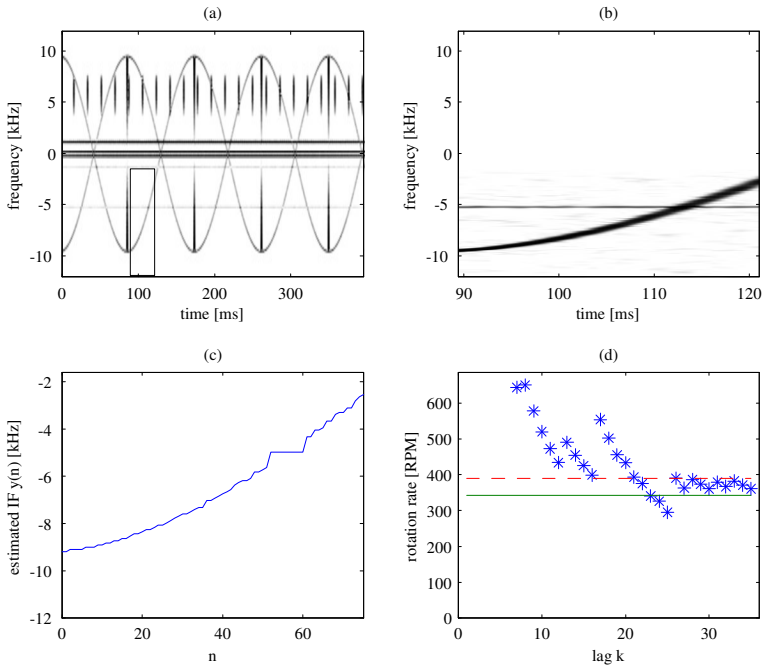

Fig. 4. (a) Time-frequency representation of the simulated helicopter data; (b) Part of the analyzed helicopter data; (c) The instantaneous frequency of the signal; (d) Estimation results for various lags k. The solid line represents the true value, asterisk represents the values estimated by method-1, and the dashed line represents the value estimated by method-2.

extracted a part of the fan data signal, which is presented in Figure 7b. The mean estimated frequency over the range of lag $6 \leq k \leq 22$ is $\hat{\omega}_e = 7.55$ Hz. The estimation method-2 gives $\hat{\omega}_2 = 6.02$ Hz. After the correction, we get $\hat{\omega}_3 = 8.08$ Hz. The true value is 7.6 Hz.

B. Rotating corner reflector

Experimental trials were conducted to investigate and determine the m-D radar signatures of targets using an X-band radar. The target used for this experimental trial was a spinning blade with corner reflectors attached that were designed to reflect electromagnetic radiation with minimal loss. These controlled experiments can simulate the rotating types of objects, generally found in an indoor environment, for example, a rotating fan and outdoor environment, for example, a rotating antenna or rotors. Controlled experiments allow us to set the desired rotation rate and then permit us to cross check and assess the results.

The blade was set up to simulate real data that might be collected from a similar target such as a rotating antenna or rotating fan or any other rotation of structures on a target. The experiment was conducted with the radar operating at 9.2 GHz. The pulse repetition frequency (PRF) was 1 kHz. The target employed in this experiment was at a range of 300 m from the radar. The S-method is utilized in order to depict the m-D oscillation.

Figure 8 illustrates the results. In this case, the rpm of the corner reflector is 28. In order to demonstrate our estimation methods, we have extracted a part of the helicopter data signal, which is presented in Figure 8b. The mean estimated frequency over the range of lag $45 \leq k \leq 64$ is $\hat{\omega}_e = 26.19$ rpm. The estimation method-2 gives $\hat{\omega}_2 = 27.09$ rpm. After the correction, we get $\hat{\omega}_3 = 28.77$ rpm. In this case, method-2 shows excellent agreement with the true value while method-1 shows reliable results at higher time lags.

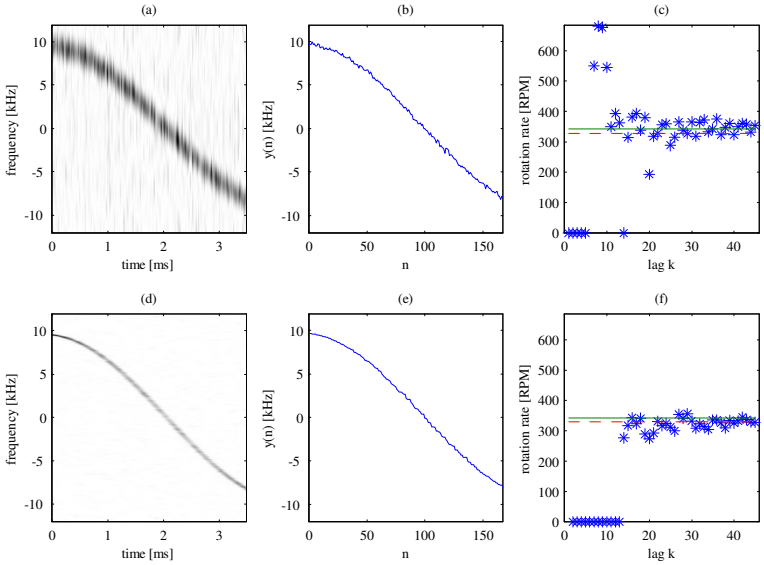

Fig. 5. Noise case using narrow window: (a) time-frequency representation of the analyzed signal, (b) the instantaneous frequency of the signal, and (c) Estimation results for various lags k. Noise case using wide window: (d) time-frequency representation of the analyzed signal, (e) the instantaneous frequency of the signal, and (f) estimation results for various lags k. The solid line represents the true value, asterisk represents the values estimated by method-1, and the dashed line represents the value estimated by method-2.

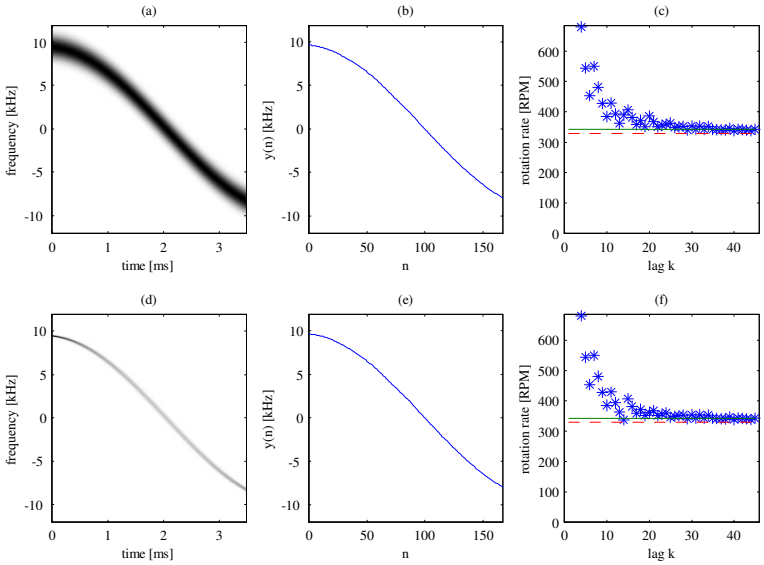

Fig. 6. Noiseless case using narrow window: (a) time-frequency representation of the analyzed signal, (b) the instantaneous frequency of the signal, and (c) estimation results for various lags k. Noiseless case using wide window: (d) time-frequency representation of the analyzed signal, (e) the instantaneous frequency of the signal, and (f) estimation results for various lags k. The solid line represents the true value, asterisk represents the values estimated by method-1, and the dashed line represents the value estimated by method-2.

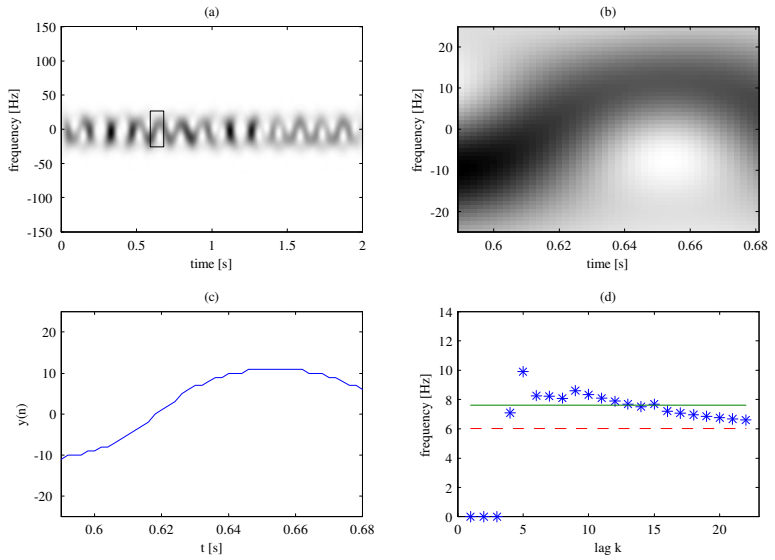

Fig. 7. (a) Time-frequency representation of the experimental fan data; (b) Part of the analyzed fan data; (c) The instantaneous frequency of the signal; (d) Estimation results for various lags k. The solid line represents the true value, asterisk represents the values estimated by method-1, and the dashed line represents the value estimated by method-2.

Figure 9 illustrates another example. In this case, the rpm of the corner reflector is 60. The mean estimated frequency over the range of lag $45 \leq k \leq 55$ is $\hat{\omega}_e = 60.65$ rpm. The estimation method-2 gives $\hat{\omega}_2 = 65.00$ Hz. After the correction, we get $\hat{\omega}_3 = 62$. In this case, method-1 shows excellent agreement with the true value.

V. Conclusion

The detection and extraction of micro-Doppler provide additional capability to better identify potential threats for security applications. Methods developed to extract micro-Doppler information for the past decade rely primarily on the assumption that the time series of the signal contains at least one oscillation or more during the coherent integration time or imaging time. However, real-world applications engage short duration signals and often require detection and estimation of micro-Doppler characteristics. Short duration signals may contain only a fraction of an oscillation. In this paper, two methods for extracting micro-Doppler oscillation parameters have been proposed. In these scenarios, the coherent integration will cover only 1/4 and 1/2 of the oscillation. The first method is based on a three-point model and the second method is based on a cubic polynomial fitting and an approximation. The reliability and robustness of these two methods are evaluated using both simulated and experimental data. Both proposed methods have shown satisfactory accuracy for both simulated and experimental data.

Results from this study show that when the number of discretization levels is high, both methods provide reliable and robust estimation of the motion parameters. When there is limited number of discretization levels, the estimation method-1 provides reliable results at higher time lags while the estimation while method-2 provides consistent results. The estimation method-2 requires more data in order to perform accurate cubic polynomial approximation. Both methods are sensitive to low SNR. Experimental results suggest that the estimation method-1 provides consistent reliable results at higher time lags compared to the estimation method-2, where the accuracy is within 5 percent error from the true value.

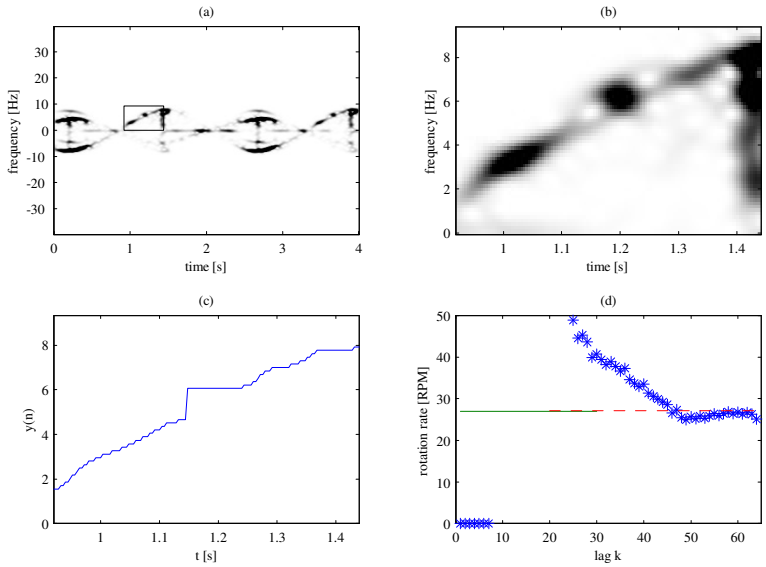

Fig. 8. (a) Time-frequency representation of the experimental corner reflector data; (b) Part of the analyzed corner reflector data; (c) The instantaneous frequency of the signal; (d) Estimation results for various lags k. The solid line represents the true value, asterisk represents the values estimated by method-1, and the dashed line represents the value estimated by method-2.

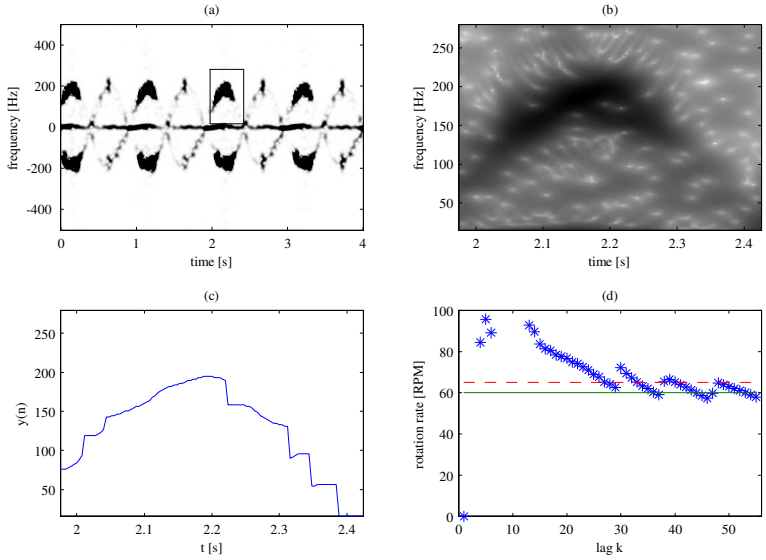

Fig. 9. (a) Time-frequency representation of the experimental corner reflector data; (b) Part of the analyzed corner reflector data; (c) The instantaneous frequency of the signal; (d) Estimation results for various lags k. The solid line represents the true value, asterisk represents the values estimated by method-1, and the dashed line represents the values estimated by method-2.

Micro-Doppler features have great potential for use in automatic target classification algorithms. Although there have been studies of m-D effects in radar in the past few years, this is the first study for micro-Doppler parameter estimation from a fraction of the period, that has great potential for use in target identification applications. As such, this paper contributes additional experimental m-D data and analysis, which should help in developing a better picture of the m-D research and its applications to indoor and outdoor radar detection and automatic gait recognition systems.

References

[1] V. C. Chen, and H. Ling, *Time-frequency transform for radar imaging and signal analysis*, *Artech House,* Boston, 2002.

[2] T. Thayaparan, S. Abrol, E. Riseborough, L. Stanković, D. Lamothe, and G. Duff. (2007), "Analysis of Radar Micro-Doppler Signatures From Experimental Helicopter and Human Data," *IEE Proceedings Radar Sonar Navig.,* 1, (4), pp. 288-299.

[3] T. Thayaparan, L. Stankovic., and I. Djurovic: "Micro-Doppler Based Target Detection and Feature Extraction in Indoor and Outdoor Environments, "*J. of the Franklin Institute,* 345, pp. 700-722, 2008.

[4] V. C. Chen, F. Li, S.-S. Ho, and H. Wechsler: "Analysis of micro-Doppler signatures," *IEE Proc. Radar, Sonar, Navig.*, Vol. 150, No. 4, Aug. 2003, pp. 271-276.

[5] V. C. Chen, F. Li, S.-S. Ho, and H. Wechsler, "Micro-Doppler effect in radar: phenomenon, model, and simulation study", Vol. 42, No. 1, pp. 2-21, *IEEE Trans. on Aerospace and Electronis Systems,*, 2006.

[6] T. Sparr, and B. Krane, "Micro-Doppler analysis of vibrating targets in SAR", *IEE Proc-Radar Sonar Navig.,* Vol. 150, No. 4, pp. 277-283, 2003.

[7] J. Li, and H. Ling: "Application of adaptive chirplet representation for ISAR feature extraction from targets with rotating parts", *IEE Proc. Radar, Sonar, Navig.*, Vol.150, No.4, August 2003, pp.284-291.

[8] T. Thayaparan, "Micro-Doppler analysis of the rotation antenna in airborne SAR image collected by the APY-6 radar," *IRS 2005*, Berlin, Germany, Sept. 2005.

[9] L. Stanković, T. Thayaparan, and I. Djurović, "Separation of target rigid body and micro-Doppler effects in ISAR imaging", *IEEE Trans. on AES,* Vol. 41, No. 4. pp. 1496-1506, 2006.

[10] P. Setlur, M. Amin, and T. Thayaparan: "Micro-Doppler signal estimation for vibrating and rotating targets," in *Proc. of ISSPA 2005*, Sydney, Austr. 2005, pp. 639-642.

[11] L. Stanković, "A method for time-frequency analysis," *IEEE Trans. Signal Process.*, Vol. 42, pp. 225-229, 1994.

[12] S. L. Marple: "Special time-frequency analysis of helicopter Doppler radar data", in *Time-Frequency Signal Analysis and Processing*, ed. B. Boashash, Elsevier 2004.

[13] B. Boashash, "Estimating and interpreting the instantaneous frequency of a signal - Part I," *Proc. IEEE*, Vol. 80, No.4, Apr. 1992, pp. 521-538.

[14] I. Djurović, and LJ. Stanković: "An algorithm for the Wigner distribution based instantaneous frequency estimation in a high noise environment", *Signal Processing*, Vol. 84, No. 3, Mar. 2004, pp. 631-643.